Communication

Selective Synthesis of CoO Nanocrystal with Different Shape and Crystal Plane Effect on Catalytic Property for Methane Combustion

Linhua Hu, Qing Peng, and Yadong Li

J. Am. Chem. Soc., **2008**, 130 (48), 16136-16137 • DOI: 10.1021/ja806400e • Publication Date (Web): 08 November 2008

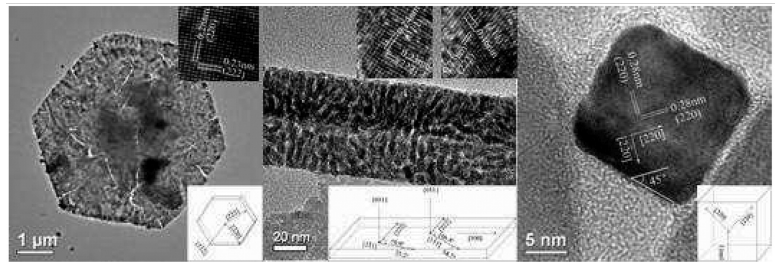

More About This Article

Additional resources and features associated with this article are available within the HTML version:

- Supporting Information
- Access to high resolution figures
- Links to articles and content related to this article
- Copyright permission to reproduce figures and/or text from this article

View the Full Text HTML

J|A|C|S
COMMUNICATIONS

Published on Web 11/08/2008

Selective Synthesis of Co_3O_4 Nanocrystal with Different Shape and Crystal Plane Effect on Catalytic Property for Methane Combustion

Linhua Hu, Qing Peng, and Yadong Li*

Department of Chemistry, Tsinghua University, Beijing, 100084, P. R. China

Received August 12, 2008; E-mail: ydli@mail.tsinghua.edu.cn

Shape and crystal plane effects of nanocrystal (NC) catalysts in different reactions have attracted remarkable attention.[1−5] The different reactivity and selectivity of catalysts depend greatly upon the different arrangement manner of surface atoms and the number of dangling bonds on different crystal planes. Transitional heterogeneous catalysts are usually composed of assorted polycrystals with different exposed crystal planes, possessing several kinds of active sites, which exhibit different reactivities and usually lower catalytic activity. Therefore, selective synthesis of differently shaped nanocrystal catalysts with uniform crystal planes under nanoscale is the important prerequisite in investigating the difference in their catalytic property.

Transition metal oxide is an important catalyst support in many catalytic reactions and serves especially as a substitute for the transitional noble catalyst in the activation of hydrocarbon.[6] Spinel cobalt oxide (Co_3O_4) represents a promising transition oxide catalyst in methane catalytic combustion, which is concentrated on composite catalysts doped with noble metal and rare earth metal oxides.[7] Differently shaped Co_3O_4 NCs such as cubes, sheets, wires, tubes,[8−12] and so forth have been synthesized via different methods, and their applications in Li ion batteries and gas sensor have been reported.[9−11] However, very little is known about Co_3O_4 NCs with different shape and crystal plane effects for methane catalytic combustion. Herein, we report controllable synthesis of Co_3O_4 with a different shape via a hydrothermal process of cobalt hydroxide precursor and subsequent thermal decomposition for methane combustion. Results show that the unusually high index {112} crystal planes of Co_3O_4 NCs are more reactive than the basic {001} and {011} planes.

Specific preparation of Co_3O_4 nanosheets, nanobelts, and nanocubes is described in the Experimental Section of the Supporting Information. The precursor of the Co_3O_4 nanosheets is the β-$Co(OH)_2$ nanosheet, whereas that of Co_3O_4 nanobelts is $Co(CO_3)_{0.5}(OH)\ 0.11H_2O$ nanobelts as shown in Figures S1, S2, and S6−S8.

Figure 1 shows representative SEM, TEM, and HRTEM images of Co_3O_4 nanosheets, nanobelts, and nanocubes. Co_3O_4 nanosheets are uniform hexagons and their average thickness and edge length is ca. 50−100 nm and 3 μm, respectively, whereas the average length and width of the Co_3O_4 nanobelts is ca. 2−5 μm and 50−100 nm. The as-prepared Co_3O_4 nanocubes are monodispersed with a uniform size of ca. 15∼20 nm. The dominant exposed planes of Co_3O_4 nanosheets are {112}, which are the only planes normal to both the set of (220) planes with a lattice space of 0.28 nm and the set of (222) planes with a square crossing lattice space of 0.23 nm. The magnified HRTEM images of selected area A, B, and C of a typical Co_3O_4 nanosheet are shown in Figure S3.

The dominant exposed planes of Co_3O_4 nanobelts are {011}, which are the only planes normal to both the first set of (311) planes with a lattice space of 0.24 nm and its corresponding set of (222) planes with a crossing lattice space of 0.23 nm, and the second set of (111) planes with a lattice space of 0.46 nm and its corresponding set of (222) planes with a crossing lattice space of 0.23 nm. The magnified HRTEM image of Co_3O_4 nanobelts is shown in Figure S4. The dominant exposed planes of Co_3O_4 nanocubes are {001}, which are the only planes normal to the set of (220) planes with a lattice space of 0.28 nm. The magnified HRTEM image of Co_3O_4 nanocubes is shown in Figure S5.

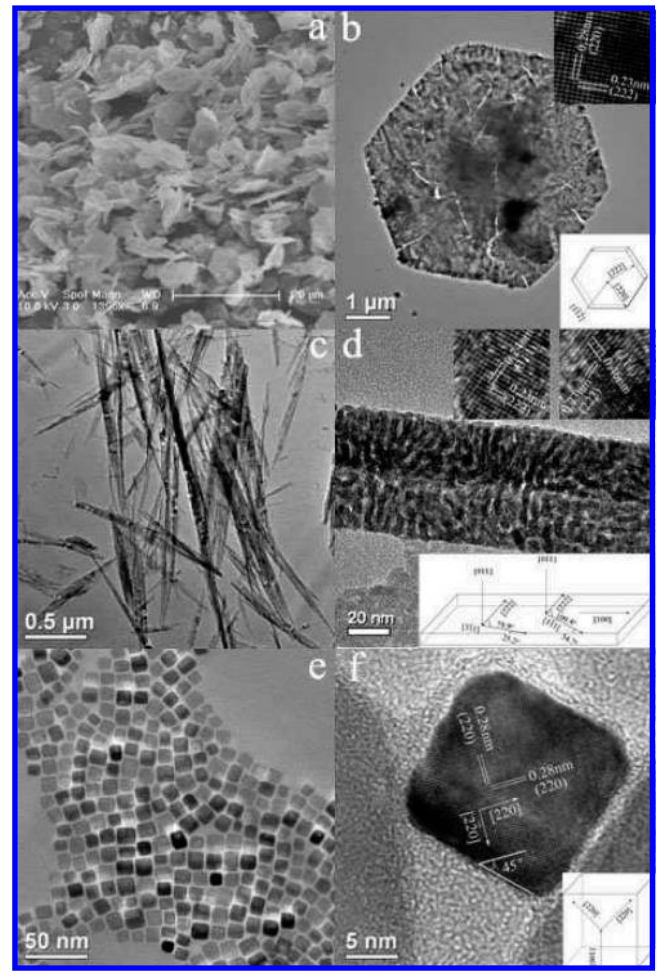

Figure 1. (a) SEM image of typical Co_3O_4 nanosheets; (b) HRTEM image and structure model of a typical Co_3O_4 nanosheet; (c) TEM image of typical Co_3O_4 nanobelts; (d) HRTEM image and structure model of a typical Co_3O_4 nanobelt; (e) TEM image of typical Co_3O_4 nanocubes; (f) HRTEM image and structural model of a typical Co_3O_4 nanocube.

All diffraction peaks of XRD patterns of Co_3O_4 nanosheets, nanobelts, and nanocubes patterns can be indexed as the fcc phase (space group *Fd3m*) and with a lattice constant $a = 8.065$ Å, which are consistent with the values in the literature (JCPDS# 74-1657) in Figure S9.

Figure 2a shows the catalytic properties of differently shape Co_3O_4 nanocrystals. When GHSV is 40 000 h^{-1}, the value of T_{50} in Co_3O_4 nanocubes is 343 °C. Compared with Co_3O_4 nanocubes, the value of

10.1021/ja806400e CCC: $40.75

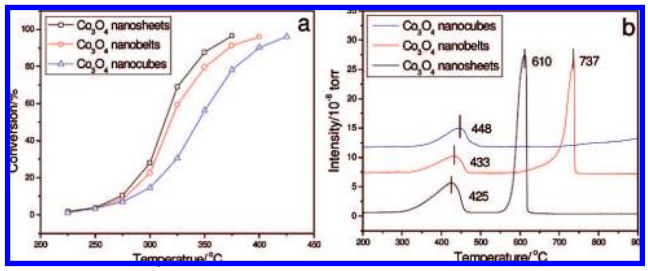

Figure 2. (a) Methane conversion as a function of temperature over Co_3O_4 nanosheets, nanobelts, and nanocubes at GHSV = 40 000 h^{-1}; (b) CH_4-TPR profiles of Co_3O_4 nanosheets, nanobelts, and nanocubes.

Scheme 1. Representation of Surface Atoms Arrangement of fcc Co_3O_4 Nanocrystal with Different Crystal Planes[a]

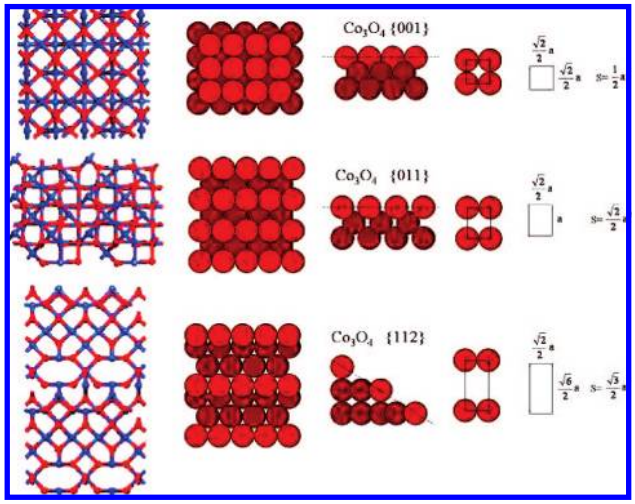

[a] The red and blue sphere is oxygen atom and cobalt atom, respectively. The brown and crimson sphere is surface layer and next layer of Co_3O_4 unit cell, respectively.

T_{50} in Co_3O_4 nanobelts shows a decrease of 24 °C, while the value of T_{50} in Co_3O_4 nanosheets shows a decrease of 30 °C. The CH_4 conversion is 50% over Co_3O_4 nanosheets, 42% over Co_3O_4 nanobelts, and 23% over Co_3O_4 nanocubes at 313 °C, with the corresponding specific rates of CH_4 conversion being 2.72, 2.28, and 1.25 μmol g^{-1} s^{-1}, respectively. The specific rate of conversion over Co_3O_4 nanosheets at 313 °C is therefore two times higher than that over nanocubes and 19% higher than that over nanobelts. The activity data show that the Co_3O_4 nanosheets are more active than Co_3O_4 nanobelts and nanocubes. However, the BET surface area of Co_3O_4 nanosheets, nanobelts, and nanocubes is 17.8, 20.1, and 22.6 m^2 g^{-1}, respectively. It indicates that the well-defined crystal plane is a significant influence factor than other interspaces within nanocrystals. The similar results are listed in Table S10 under other conditions. The three Co_3O_4 NCs are stable in a 300 h test when the CH_4 conversion is ca. 94−98%.

Figure 2b shows the CH_4-TPR profiles of Co_3O_4 nanosheets, nanobelts, and nanocubes obtained by monitoring the product CO_2. For Co_3O_4 nanosheets, the broader peak centered at 425 °C and the narrower peak centered at 610 °C can be attributed to the reduction process of Co^{3+} to Co^{2+} (step I) and Co^{2+} to Co^0 (step II), respectively, while for Co_3O_4 nanobelts, the reduction peak of step I and step II shifts to 433 and 737 °C, respectively. However, for Co_3O_4 nanocubes, there is one peak centered at 448 °C of step I without step II. On the other hand, the as-formed amount of CO_2 over Co_3O_4 nanosheets is larger than that of nanobelts and nanocubes. This indicates that Co_3O_4 nanosheets show a stronger redox property than Co_3O_4 nanobelts and nanocubes. The detailed analysis of CH_4, H_2O, CO, and H_2 is shown in Figure S11.

Scheme 1 shows the representative surface atoms arrangement of the fcc Co_3O_4 nanocrystal with different crystal planes. The area of adjacent four brown spheres of the {001}, {011}, and {112} planes is $(^1/_2)a^2$, $(\sqrt{2}/2)a^2$, and $(\sqrt{3}/2)a^2$, respectively, suggesting the {112} plane is more open than the {001} and {011} planes. Therefore, the {112} planes have a more reactive surface. On the other hand, the number of missing neighbors of a unit cell in {001}, {011}, and {112} planes is 4, 5, and 5, respectively. Therefore, the difference of catalytic property between the {011} and {112} planes is smaller than that between the {001} and {011} planes. The magnified slab model of surface atoms is shown in Figure S12.

In summary, Co_3O_4 nanosheets, nanobelts, and nanocubes have been successfully synthesized via a hydrothermal process of cobalt hydroxide precursor and subsequent direct thermal decomposition. The predominantly exposed planes are {112} in the Co_3O_4 nanosheets, {011} in the Co_3O_4 nanobelts, and {001} in the Co_3O_4 nanocubes, respectively. The catalytic activity order for methane combustion of these crystal planes follows {112} > {011} ≫ {001}. We believe that this approach, which is based on the predictable choice of shape and crystal plane, can be readily extended to the synthesis of other related transition oxides with similar nanocatalytic systems including nanowires, nanorods, and nanoparticles, when at least one of the material's dimensions is reduced to the nanoscale. The selective synthesis of transition metal oxides with uniform and different reactive crystal planes at nanoscale is expected to bring up new opportunities for design, tuning, and control of chemical activity, specificity, and selectivity.

Acknowledgment. This work was supported by NSFC (90606006) and the State Key Project of Fundamental Research for Nanoscience and Nanotechnology (2006CB932303). Thanks Prof. Li Jun of Tsinghua University, Prof. Ji Shengfu of Beijing University of Chemical Technology, and Dr. Yu Changchun of China University of Petroleum for the helpful discussion.

Supporting Information Available: SEM images, TEM images, XRD patterns of cobalt hydroxide precursor and cobalt oxide, stability of catalysts, CH_4-TPR profiles. This material is available free of charge via the Internet at http://pubs.acs.org.

References

(1) Burda, C.; Chen, X.; Narayanan, R.; El-Sayed, M. A. *Chem. Rev.* **2005**, *105*, 1025.
(2) Zhou, K. B.; Wang, X.; Sun, X. M.; Peng, Q.; Li, Y. D. *J. Catal.* **2005**, *229*, 206.
(3) Zhang, Y. W.; Grass, M. E.; Habas, S. E.; Tao, F.; Zhang, T. F.; Borodko, Y. R.; Yang, P. D.; Somorjai, G. A. *Abstracts of Papers*, 234th ACS National Meeting, Boston, MA, United States, August 19−23; American Chemical Society: Washington, DC, **2007**; INOR-138.
(4) Tian, N.; Zhou, Z. Y.; Sun, S. G.; Ding, Y.; Wang, Z. L. *Science* **2007**, *316*, 732.
(5) Si, R.; Flytzani-Stephanopoulos, M. *Angew. Chem., Int. Ed.* **2008**, *47*, 2884.
(6) (a) Yin, F. X.; Ji, S. F.; Chen, B. H.; Zhao, L. P.; Liu, H.; Li, C. Y. *Appl. Catal., B* **2006**, *66*, 265. (b) Lee, J. H.; Trimm, D. L. *Fuel Process. Technol.* **1995**, *42*, 339. (c) Choudhary, T. V.; Banerjee, S.; Choudhary, V. R. *Appl. Catal., A:* **2002**, *234*, 1.
(7) (a) Li, Z. H.; Hoflund, G. B. *React. Kinet. Catal. Lett.* **1999**, *66*, 367. (b) Liotta, L. F.; Carlo, G. D.; Pantaleo, G.; Deganello, G. *Catal. Commun.* **2005**, *6*, 329. (c) Liotta, L. F.; Carlo, G. D.; Pantaleo, G.; Veneziaa, A. M.; Deganello, G.; Merlone Borla, E.; Pidriac, M. F. *Top. Catal.* **2007**, *42*−*43*, 425. (d) Liotta, L. F.; Carlo, G. D.; Pantaleo, G.; Deganello, G. *Appl. Catal., B* **2007**, *70*, 314.
(8) (a) Xu, R.; Zeng, H. C. *J. Phys. Chem. B* **2003**, *107*, 926. (b) Ji, F.; Zeng, H. C. *Chem. Mater.* **2003**, *15*, 2829. (c) He, T.; Chen, D. R.; Jiao, X. L.; Wang, Y. L.; Duan, Y. Z. *Chem. Mater.* **2005**, *17*, 4023.
(9) (a) Li, Y. G.; Tan, B.; Wu, Y. Y. *J. Am. Chem. Soc.* **2006**, *128*, 14258. (b) Li, Y. G.; Tan, B.; Wu, Y. Y. *Nano Lett.* **2008**, *8*, 265.
(10) Lou, X. W.; Deng, D.; Lee, J. Y.; Feng, J.; Archer, L.A. *Adv. Mater.* **2008**, *20*, 258.
(11) Li, W. Y.; Xu, L. N.; Chen, J. *Adv. Funct. Mater.* **2005**, *15*, 851.
(12) Li, L. L.; Chu, Y.; Liu, Y.; Song, J. L.; Wang, D.; Du, X. W. *Mater. Lett.* **2008**, *62*, 1507.

JA806400E